

Article

CQDs@NiO: An Efficient Tool for CH₄ Sensing

Marilena Carbone 

Department of Chemical Science and Technologies, University of Rome Tor Vergata, Via della Ricerca Scientifica 1, 00133 Rome, Italy; marilena.carbone@roma2.infn.it or carbone@uniroma2.it

Received: 11 August 2020; Accepted: 4 September 2020; Published: 9 September 2020



Featured Application: The composite material made of CQDs on NiO surface can be used as sensing material in CH₄ detection. As show-case a home-made CH₄ sensor has been built, based on the CQDs@NiO.

Abstract: A composite material based on carbon quantum dots (CQDs) and NiO was prepared and tested for methane sensing. The synthesis procedure is simple and foresees the preparation of the CQDs by citric acid pyrolysis and NiO by hydrothermal synthesis. A phase sonication and stirring procedure yielded the composite CQDs@NiO at different loads. The composites were characterized by X-ray diffraction, ultraviolet–visible light (UV–Vis) spectroscopy, SEM microscopy, energy-dispersive spectroscopy (EDS) mapping, and surface area, porosity, and impedance measurements. A gas sensor was built in-house and used to probe the response of the synthesized samples to CH₄ detection, at constant environmental humidity. The CQDs@NiO at 1% weight load displayed excellent performances in terms of gas response both vs. temperature and vs. concentration, whereas higher loads resulted in CQD aggregation and diminished output. Response/recovery times of the 1%CQDs@NiO sample were good, as well as the selectivity and the stability over time and for variable environmental humidity. The estimated limit of detection was 0.1 ppm.

Keywords: NiO; carbon quantum dots; methane sensing; moist environments

1. Introduction

Methane gas is extensively employed as fuel in houses and industries, and as a propellant for automotive vehicles [1–3]. As a chemical raw material, it also finds application in the production of carbon black, acetylene, carbon disulfide, and methanol [4], among others. CH₄ is the main gas component in coal mines, and it is extremely dangerous, since it easily explodes when it reaches a volume concentration between 4.9% and 15.4% in air. Because of the odorless and flammable nature of this asphyxiant gas, the development of sensitive detectors for real-time detection at concentrations lower than its explosive limit is in pressing need. Furthermore, low-cost fabrication of CH₄ sensors is an asset in order to make such devices easily accessible to the general public. In this framework, the ideal combination of sensors properties includes sensitivity, quick response, low-cost sensing material and sensor components. Platforms such as the electrochemical ones, which often proved to be effective toward multiple targets [5–12], were also applied to CH₄ sensing [13–15], which required the gas being trapped in liquids. It must be added that, for other gases such as CO₂, potentiometric sensors were developed, without a need for trapping in liquid, albeit working at high temperatures and requiring a BaCO₃ layer for limiting the humidity interference [16]. Under these premises, we designed and probed a low-cost material to insert in a home-assembled sensor, built with an easily available set of components, for high-sensitivity CH₄ detection. The rationale in the approach for defining the sensing material is the best match of substrate and additional modifying material to enhance the sensing properties. We opted for NiO as a substrate, because of its good sensing

properties toward CH₄ [17], and because it can be synthesized in different morphologies and various surface areas and porosity [18–20], with the aid of several synthetic techniques [21–23], whereby the morphological properties reflect the gas-sensing performance [24–27]. Furthermore, it was shown it can be successfully modified to further improve its sensing capabilities [28]. In general, several variants of NiO-based materials have been proposed, as sensing elements of gases, with different morphologies, doping, and p-n junction constructions conditioning the sensing properties. Recently, nanocrystalline NiO nanoplates [29], porous NiO nanosheets [30], and Pt@NiO core-shell nanostructure [31] were employed in hydrogen sensing. Selective sensitivity toward NO₂ in a humid environment was confirmed by the limited response for different reducing gases, such as CO, CH₄, NH₃, and SO₂, using ultrathin NiO sensors [32]. Acetone could be detected using Ru-doped NiO [33] or NiFe₂O₄ nanoparticle-decorated NiO nanosheet sensors [34]. Detectors for toluene [35], formaldehyde [36], triethylamine [37], xylene [38], methanol [39], and ethanol [24,40] were implemented, using NiO heterojunctions, porous NiO, NiO nanoparticles, nanoplatelets, and decorated NiO. The modifications put in place for methane detection so far are largely based on the improvement of the response properties by creating nanocomposites such as NiO-rGO (reduced graphene oxide) [28] and hetero-junctions [41] with p-type NiO. As far as methane detection is concerned, sensors are often based on n-type semiconductors, and SnO₂ is typically used. Recently, Pd-SnO₂ [42], Pt-SnO₂ [43], and r-GO/SnO₂ [44] were investigated as materials for methane sensors. On the other hand, SnO₂ was also used by decorating NiO for the same sensing purpose [45]. In terms of performance, these sensor materials display optimum working temperatures in the range 150–340 °C for detection of 100 to 1000 ppm CH₄.

In the present investigation, to accredit practical, low-cost, efficient solutions, we successfully modified NiO with carbon quantum dots (CQDs) to augment the NiO response with a carbon material which can uniformly spread over surfaces and pores and create a homogeneous network. Among all possible solutions, CQDs appeared to be a very convenient option as they can be easily obtained by pyrolysis of any carboxylic acid [46] alone or in combination with other pyrolysis-sensitive components such as Tris-HCl [47]. Although primarily and extensively used as fluorescent probes in metal detection and cell labeling [48], CQDs proved to be a remarkable modifier of NiO, achieving high CH₄ detection performance.

The novelty of this paper is the improvement of the response toward CH₄ sensing both by playing on the NiO morphology and by employing CQDs. This creates edges and grain boundaries where the methane molecules react with oxygen and, via CQD sheathing, aiding the electronic processes in chemoresistive detection [49]. The electronic properties of CQDs were explored by Bhattacharjee et al. [50] who synthesized poly(4-styrene sulfonate)-stabilized carbon quantum dots via citric acid pyrolysis and deposited them on an ITO (indium tin oxide) surface. In general, CQDs are effective for their electrocatalytic properties [51], with conductive polymers sometimes playing a role [52].

In the present paper, CQDs@NiO were achieved via separate synthesis of the NiO substrate and CQDs, followed by mixing via phase sonication and stirring. A sensing platform was constructed to allow sensitive detection and simultaneous monitoring of the ambient parameters (humidity and temperature), employing low-cost commercial components and open-access software. One of the most overlooked aspects when testing sensor performance is the moisture resistance. On the other hand, the CQDs@NiO could be applied to reduce the influence of environmental humidity. Upon optimization of the operational parameters, it turns out that the synthesized composite material has very good performance in CH₄ sensing, in humid environments, with a high selectivity, where the best performance was achieved by the 1%CQDs@NiO, i.e., the sensor built using NiO with 1% weight load of CQDs. As compared to SnO₂-based sensors [28,41–45], the optimum temperature of the 1%CQDs@NiO sensor is equal or lower (150 °C), with detection of a lower concentration of CH₄. The response/recovery time is on average lower (with the exception of the Pd-SnO₂-based sensor [42]). Altogether, the combination of response parameters is improved with respect to previous sensors, and the gas response expressed as R_g/R_a (gas resistance vs. air resistance) is higher. Furthermore,

this type of sensor has the advantage of a facile synthesis using low-cost materials. Conversely, since the performance is largely dependent on the amount of CQDs, it may require some effort to tune the synthesis toward the best working composition.

2. Materials and Methods

2.1. Synthetic Procedure

The NiO sample was prepared via a hydrothermal route, by adding 50 mL of 1.2 mol·L⁻¹ (NH₂)₂CO dropwise to 50 mL of 0.6 mol·L⁻¹ Ni(NO₃)₂, at room temperature, under vigorous stirring. The pH was adjusted to 8.0 using HNO₃. The suspension was then transferred into a 200 mL Teflon-lined stainless-steel autoclave, carefully sealed, and heated at 180 °C for 24 h in a furnace. After gentle cooling, the powder was repeatedly washed with deionized water and dried at 60 °C overnight. The powder was then placed in a tubular oven and heated at a rate of 10 °C/min to 500 °C, and then calcined for 3 h. CQDs were synthesized by pyrolyzing 2 g of citric acid (CA) in a round-bottom flask, immersed in an oil bath at 200 °C for 30 min. The yellow-orange liquid supplemented with deionized water, up to a volume of 50 mL. Quotas of 0.5 mL, 1 mL, and 1.5 mL of the CQD solutions were each supplemented with 2 g of NiO and brought to 5 mL using deionized water. The dispersions of NiO in CQD aqueous solutions were subjected to phase sonication and stirring, i.e., cycles of 10 min sonication in a 40 kHz bath followed by room temperature stirring at 1000 rpm. The deposition of the yellow-orange CQDs from the aqueous solution to the NiO surface resulted in the depletion of the colored material from the solution, which was, as a consequence, discolored. Therefore, the phase sonication procedure was deemed complete when the discoloration of the solution took place. The samples were centrifuged at 3000 rpm and then dried overnight at 80 °C. They were then labeled 1%CQDs@NiO, 2%CQDs@NiO, and 3%CQDs@NiO, reflecting the ratio by weight of CA vs. NiO.

2.2. Materials and Equipment

Citric acid (CA), Ni(NO₃)₂, (NH₂)₂CO, ethanol, and acetone were purchased from Sigma-Aldrich (Sigma-Aldrich, St. Louis, Missouri, USA). All chemicals were of reagent grade and used without any further purification. The samples were characterized by X-ray diffraction (XRD), using an X' pert pro X-ray diffractometer by Philips (Almelo, The Netherlands), operated with CuK-Alpha radiation. Ultraviolet–visible light (UV–Vis) spectra were acquired using a Varian Cary 50 Scan spectrophotometer (Agilent, Santa Clara, USA). SEM images were acquired with a Zeiss Auriga field-emission scanning electron microscope instrument (Jena, Germany) operating at 7 kV. The energy-dispersive spectroscopy (EDS) maps were obtained by coupling the field-emission scanning electron microscope (SUPRA™ 35, Carl Zeiss SMT, Oberkochen, Germany) with energy-dispersive microanalysis (EDS/EDX, INCAx-sight, Model: 7426, Oxford Instruments, Abingdon, Oxfordshire, UK), operating at 20 kV. High-resolution transmission electron microscopy (HR-TEM) was performed on an FEI Tecnai G2 20 high-resolution transmission electron microscope (FEI Company, Hillsboro, USA). The specific surface area and porosity were measured on Micrometrics Instrument Corporation ASAP 2020 (Norcross, Georgia, USA) using N₂ adsorption–desorption isotherms. The methane sensor was assembled according to the scheme in Figure S1 (Supplementary Materials). It allows resistive gas response as a function of temperature and concentration, simultaneously keeping record of the ambient conditions (external temperature and humidity). CQDs@NiO powders were ground in an agate mortar, mixed with deionized water in a ratio of 5:1 until a paste was formed, and then coated onto the ceramic support, which was then connected to four Pt wires through two Au rings. The coated ceramic elements were then dried at 200 °C for 5 h in air for water to evaporate and to ensure stability. The thickness of the coating was 200 nm. The sensor was placed in a chamber of 1 L of volume with its own heating system and temperature control. Synthetic air (Sigma-Aldrich), supplemented with saturated vapor of distilled water, was used both as reference and as diluting gas. All measurements of gas response were made at

a relative humidity (RH) of 20%, unless stated otherwise. The resistance was then measured with a signal-to-noise ratio of about 4% at the minimum level and about 2% at the maximum level.

3. Results and Discussion

The achievement of the composite CQDs@NiO was evaluated in several ways. The synthesis of CQDs via CA pyrolysis yielded the typical UV–Vis spectrum with a maximum absorption at 352 nm [42], as reported in Figure 1A. The NiO sample and the composites were analyzed by X-ray diffraction, as shown in Figure 1B. NiO presented diffraction peaks at $2\theta = 37.4^\circ$, 43.4° , 63.0° , 75.5° , and 79.6° which were assigned to the (111), (200), (220), (222), and (311) reflections, respectively, pointing to a pure phase [53].

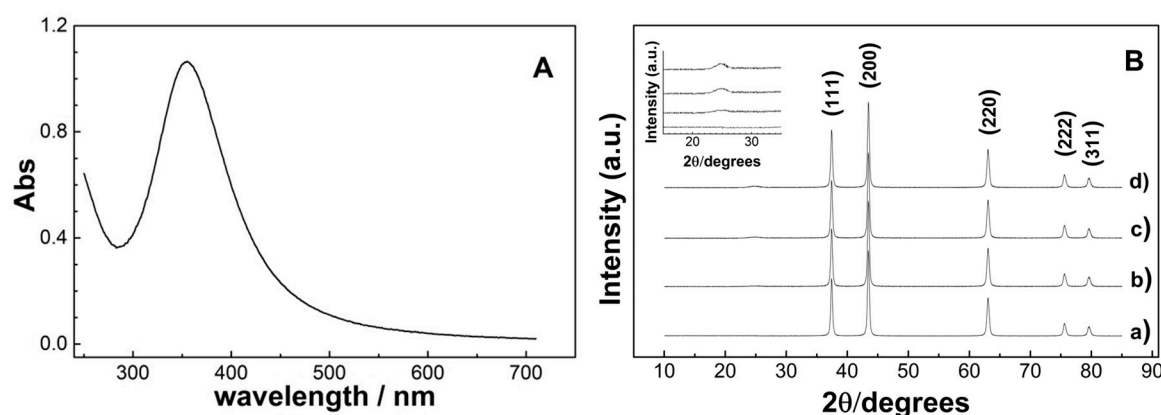


Figure 1. (A) Ultraviolet–visible light (UV–Vis) spectrum of the carbon quantum dots (CQDs); (B) X-ray diffraction (XRD) of NiO and composite samples: (a) pure NiO, (b) 1% CQDs@NiO, (c) 2% CQDs@NiO, and (d) 2% CQDs@NiO. The inset is a magnification of the 2θ region of $25\text{--}35^\circ$.

The average particle size was estimated by analysis of the peak's full width at half maximum (FWHM) using the Scherrer formula $D = K \lambda / \beta \cos(\theta)$, where K is a constant (ca. 0.9), λ is the X-ray wavelength used to collect the XRD patterns (i.e., 1.5418 \AA), θ is the Bragg angle, and β is the pure diffraction broadening of a peak at half-height due to the crystallite dimensions, yielding an appraised value of 35 nm.

From the morphological point of view, NiO synthesized via urea and nickel nitrate and calcined at 500°C has a peculiar texture of polygonal-shaped nanoparticles, with an average size of 40 nm, which tend to merge to yield a sort of bidimensional extended structure (Figure 2(a1)).

The texture was retained by adding 1% CQDs, although the porosity appeared affected to some extent. The 2% CQDs, and 3% CQDs samples still retained the polygonal-shaped structure, but the deposition of the CQDs definitively helped the merging of the nanoparticles, resulting in an extended structure (Figure 2(b1–d1)).

This reflects the distribution of the carbon on the NiO surface as mapped by EDS and shown in Figure 2(b2–d2), which was quite homogeneous for the composite 1% CQDs and had scattered islands in the 2% CQDs and 3% CQDs composites. The typical TEM image of the synthesized NiO is shown in Figure 2(c1). The corresponding HRTEM image is presented in Figure 2(b1), where an interplanar spacing of 0.208 nm was measured from the fringe pattern, corresponding to the (200) plane. From Figure 2(b3–d3), it can be found that the CQDs were homogeneously distributed onto the NiO surface in the 1% CQDs sample (round dots embedded in the NiO structure), and that their density increased in the 2% CQDs sample and tended to merge in the 3% CQDs sample.

Surface area, average pore size, and total pore volume measurements were in line with the structure and morphology analysis (see Table 1). The surface and pore parameters of NiO were slightly modified by the presence of 1% CQDs, resulting in a small reduction of the average pore size and increase of the surface area. A higher load of QDs resulted in a partial pore occlusion and reduced

surface area as expected for a more consistent deposition of the QDs into the pores and an aggregation of the quantum dots. A higher load resulted in a more pronounced effect.

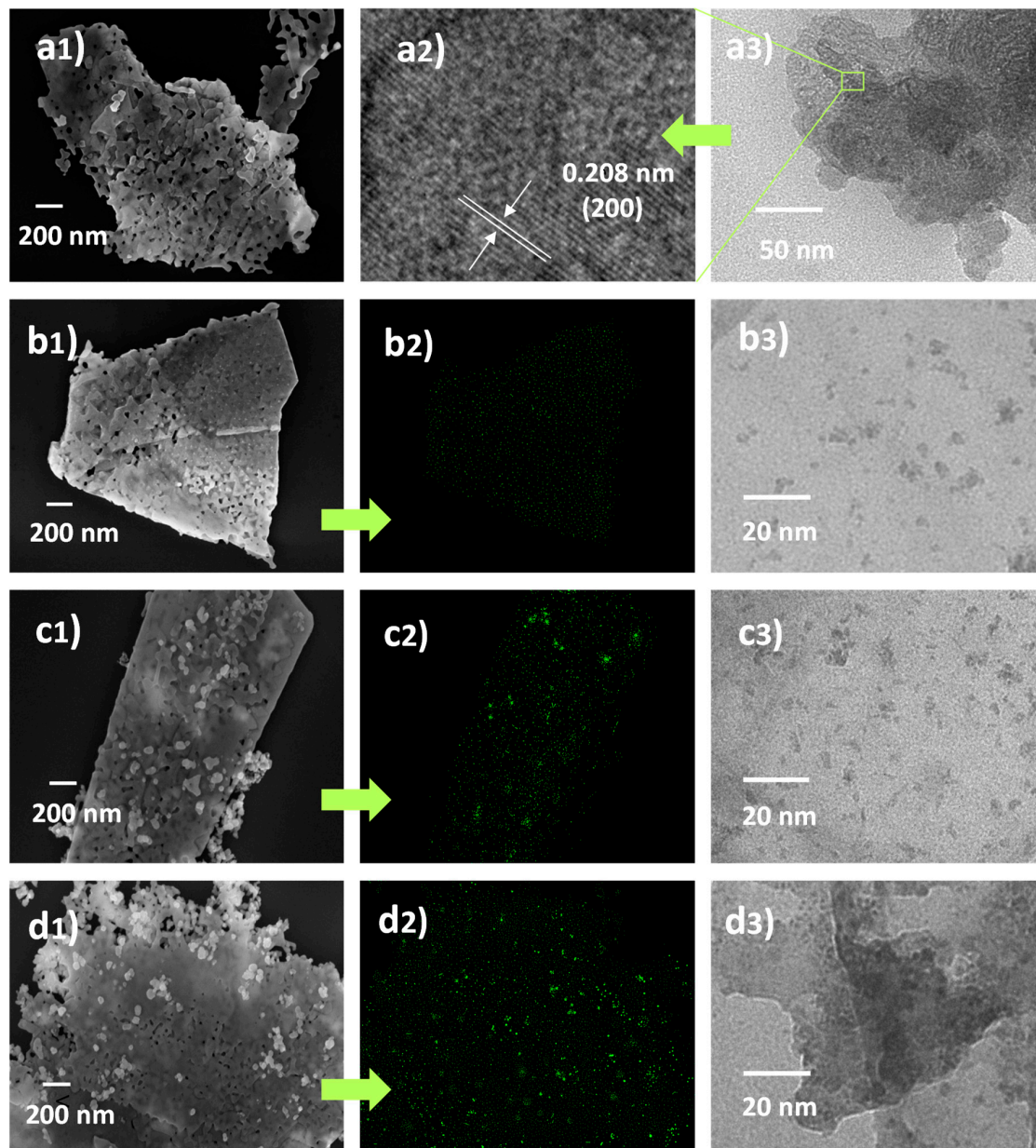


Figure 2. SEM images of (a1) NiO, (b1) 1% CQDs@NiO, (c1) 2% CQDs@NiO, and (d1) 3% CQDs@NiO. Energy-dispersive spectroscopy (EDS) carbon distribution maps of (b2) 1% CQDs@NiO, (c2) 2% CQDs@NiO, and (d2) 3% CQDs@NiO. TEM images of (a2) NiO, high-resolution (HR)-TEM, (a3) NiO, (b3) 1% CQDs@NiO, (c3) 2% CQDs@NiO, and (d3) 3% CQDs@NiO.

Table 1. Surface area, average pore size, and total pore volume of the synthesized samples.

Sample	Surface Area ($\text{m}^2 \cdot \text{g}^{-1}$)	Average Pore Size (nm)	Total Pore Volume ($\text{cm}^3 \cdot \text{g}^{-1}$)
NiO	186.7	18.6	0.53
1% CQDs@NiO	196.3	18.3	0.56
2% CQDs@NiO	156.2	15.4	0.43
3% CQDs@NiO	146.1	12.5	0.32

NiO and the composites were probed as sensing materials in CH₄ by measuring the resistivity variations, i.e., R_g/R_a (R_g = gas resistance, R_a = air resistance) as a function of operational temperature and gas concentration at an RH of 20% (Figure 3). In Figure 3a the gas response of the probed materials is reported as a function of temperature. The optimal value was 175 °C for pristine NiO and 150 °C for the composites. Previous NiO-based sensors for methane detection worked at optimum temperatures of 200 °C (ultra-thin NiO [17]), 250 °C (rGO-NiO [28]), and 330 °C (SnO₂-NiO [45]), which in all cases are higher than in the current work. This optimum temperature is also lower or, at best, equal to the working temperature of SnO₂-based sensors [41–43]. The 1%CQDs@NiO and 2%CQDs@NiO composites also displayed a larger R_g/R_a ratio than pristine NiO, whereas the highest loaded composite 3%CQDs@NiO displayed the worst performance.

Further analyses were carried out on the best-performing composite, i.e., the 1%CQDs@NiO. In Figure 3b, the gas response vs. concentration is reported for detection at 150 °C, in the range 5–50 ppm, showing a reasonably linear response (the R² coefficient of the linear regression is 0.99). In the inset, the error bars of the measurements are reported. The detection range is very good, since most of the proposed devices detect CH₄ in higher concentration ranges, whereas it is desired to be capable of detecting even small gas leaks. From the slope of the linear fit, it is possible to estimate to the limit of detection (LOD) as:

$$\text{LOD} = 3 \frac{\text{rms}_{\text{noise}}}{\text{slope}}, \quad (1)$$

where *rms_{noise}* and *slope* are the root-mean-square error of the baseline and the slope value of the linear curve [27]. For the 1%CQDs@NiO sensor, we appraised an LOD of 0.1 ppm. Figure 3c demonstrates the dynamic response and recovery curve of the 1%CQDs@NiO to 20 and 30 ppm CH₄ at 150 °C. The sensor response increased dramatically when CH₄ gas was injected into the test chamber and was swiftly recovered to the initial resistance when the sensor was exposed to air. The time taken by the sensor to reach 90% of the total resistance change is defined as the response time in the case of gas adsorption, whereas the recovery is the time needed for the specular gas desorption process [54,55]. The response and recovery times of the NiO sensor toward 30 ppm CH₄ were calculated to be about 10 s and 14 s, respectively. The performance of the 1%CQDs@NiO composite-based sensor is compared to previously reported data in Table 2. The reproducibility of the 1%CQDs@NiO-based sensor measurements is reported in Figure S2 (Supplementary Materials).

Table 2. Comparison of methane sensor characteristics in this work to recent studies. UT = ultra-thin. rGO = reduced graphene oxide. The response of p-type sensors is presented as R_g/R_a, while the n-type sensor response is presented as R_a/R_g, where R_g = gas resistance, and R_a = air resistance.

Sensing Element	Methane (ppm)	Temp (°C)	Gas Response R _g /R _a	Gas Response R _a /R _g	Response/Recovery Time (s)	Reference
1%CQDs@NiO	30	150	77.3		10/14	This work
UT-NiO	30	200	~50		15/20	[17]
rGO-NiO	1000	250	15		6–18/16–20	[28]
rGO-SnO ₂	1000	150		47.6	61/330	[44]
Pd-SnO ₂	100	340		4.38	3/5	[42]
2.5-Pt/SnO ₂	500	100		1.98	–	[43]
SnO ₂ -NiO	500	330	15.2		28/44	[45]

The stability of the 1%CQDs@NiO sensor over time was probed by testing the response to 30 ppm CH₄ at 150 °C in a time span of three weeks, revealing a rather constant behavior (Figure 3d). The effect of the relative humidity on the 1%CQDs@NiO sensors was probed by monitoring the response to 30 ppm CH₄ at 150 °C as a function of increasing RH (Figure 3d). The sensor maintained an excellent CH₄-sensing performance with little response loss in a high-RH environment due to the increased oxidation reaction facilitated by the CDQ decoration of the NiO (Figure 3e). Finally, the selectivity of

the 1%CQDs@NiO sensor was evaluated by investigating the comparative response to four target gases (CH_4 , CO_2 , NH_3 , and acetone) at 30 ppm concentration, operating at 150 °C. The results are shown in Figure 3f and indicate a marked selectivity toward CH_4 , with poor responses to the other gases.

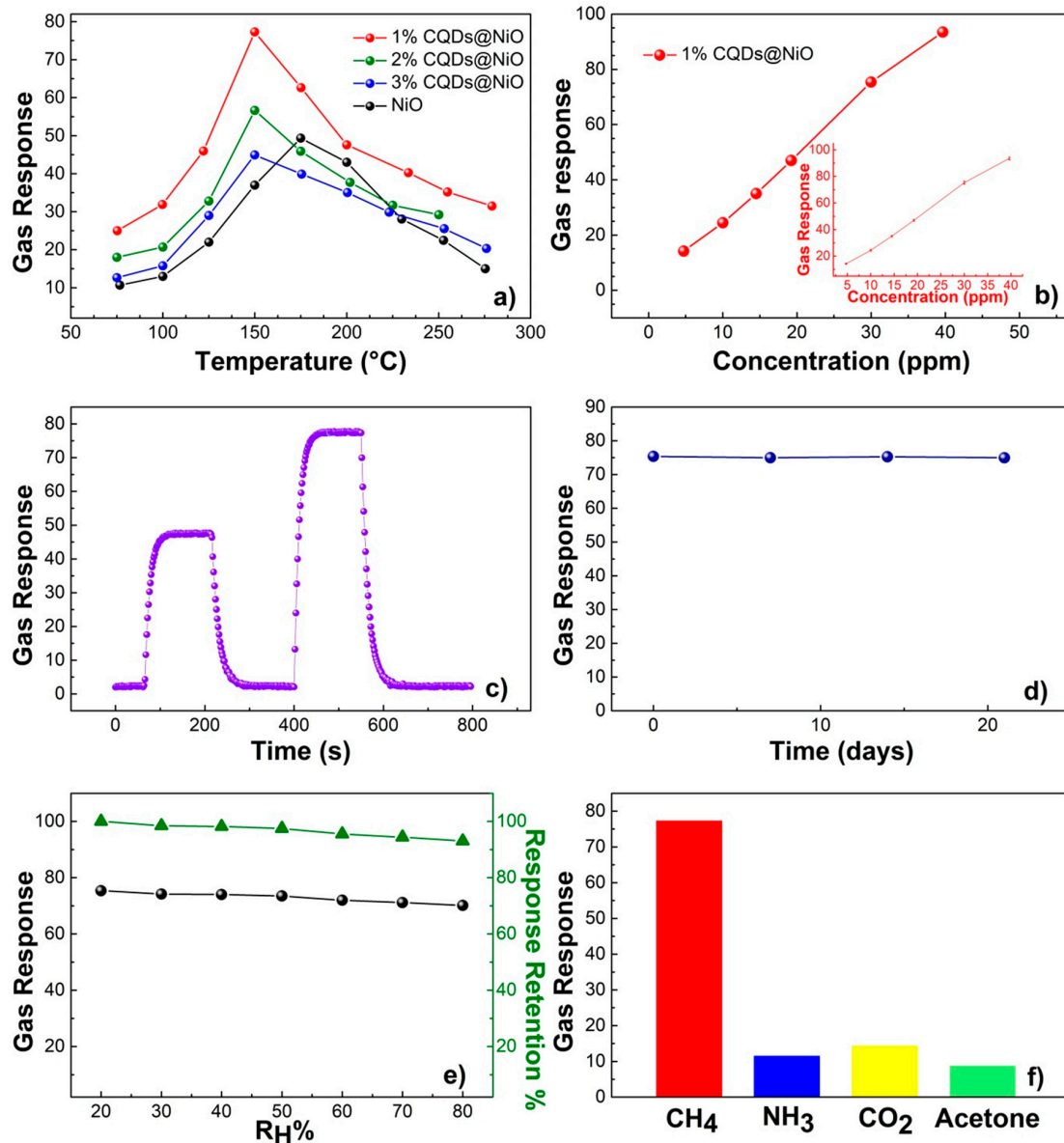
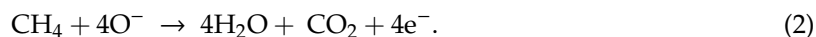


Figure 3. Gas responses of the sensing elements, defined as R_g/R_a , where R_g is the gas resistance and R_a is the air resistance: (a) gas response to 30 ppm CH_4 as a function of temperature—red dotted line (••) 1% CQDs@NiO, green dotted line (••) 2% CQDs@NiO, blue dotted line (••) 3% CQDs@NiO, black dotted line (••) NiO; (b) gas response of 1% CQDs@NiO operated at 150 °C and R_H 20%; in the inset, the same plot is presented with the error bars of the measurement and without symbols; (c) response and recovery curves of 1% CQDs@NiO at 20 ppm and 30 ppm, R_H 20%; (d) gas response of 1% CQDs@NiO to 30 ppm CH_4 over three weeks, R_H 20%; (e) gas response of 1% CQDs@NiO to 30 ppm CH_4 as a function of relative humidity (black dotted line (••) and percentage of response retention (green line with triangles ▲); (f) selectivity of 1% CQDs@NiO, operated at 150 °C and exposed to 30 ppm of the indicated gases ($R_H = 20\%$).

The detection mechanism is based on the reaction between CH₄ and adsorbed oxygen according to Equation (2).



The first step of the overall process is the adsorption of O₂ by reduction on the surface to O[−], with formation of a hole accumulation layer (HAL) related to electrostatic interaction of opposite charges [56]. In this regard, the morphology plays a role, since the edges of the polygonal-shaped structure of the NiO nanoparticles may be efficient in capturing O₂. The effects of the deposition of the CQDs on NiO can be reconducted to the formation of a hetero-junction potential barrier at the interface between CQDs and NiO, which greatly facilitates the adsorption and diffusion of the methane molecule [28,57]. More in detail, the deposition of CQDs on the NiO causes an increase in resistance following the electron–hole equilibration at the interface. On the other hand, the interface between CQDs and NiO junctions is a source of defects which are potential gas adsorption sites. Therefore, a larger number of gas molecules may adsorb and react at the interface, resulting in a decreased thickness of the HAL and higher resistance of the CQDs–NiO as compared to pure NiO sensor. By the time the chemical reaction is accomplished, electrons flow from the CQDs to NiO, which results in a further decrease of the hole concentration in NiO and even larger resistance [58,59]. Furthermore, an electrocatalytic effect may take place [60] through methane activation. The detection mechanism, then, occurs via a redox reaction between O[−] and CH₄ and injection of electrons into the solid, with a depletion of the HAL and an increase of the resistance (Figure 4) [29]. The efficiency of the detection mechanism is negatively affected by the CQD aggregation, with a consequent worsening of the detection performance at higher loads.

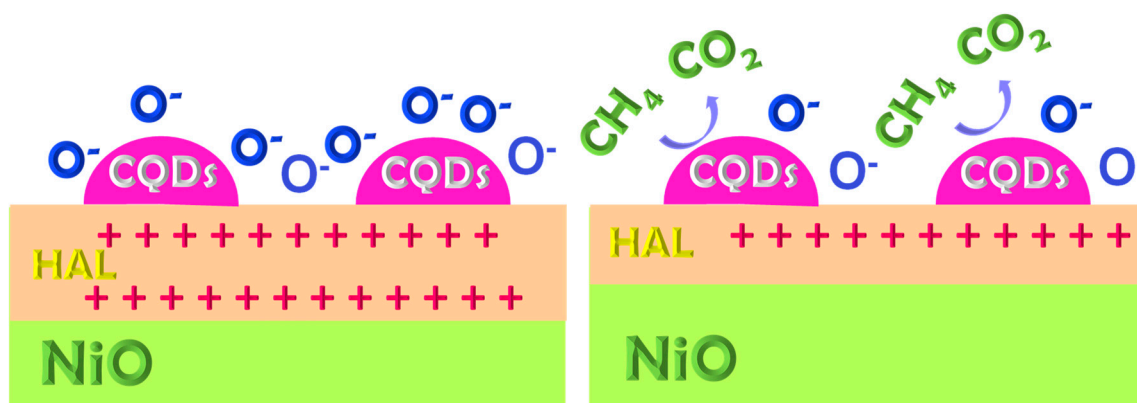


Figure 4. Detection mechanism of CH₄.

4. Conclusions

A new composite material was prepared using CQDs and NiO. The synthetic procedure is quite straightforward and foresees the separate achievement of the CQDs and of the NiO and the combination of the two by phase sonication and stirring. Composites at different loads were, then characterized, indicating a good dispersion of the CQDs on the NiO at the lowest load and partial reaggregation at higher loads. The sensing properties of the composite material toward CH₄ were probed using a low-cost, home-made device and parallel the dispersion of the CQDs on NiO. The lowest loaded sample shows the best performance in terms of operational temperature. Furthermore, it has an estimated LOD of 0.1 ppm and a good response/recovery time, is stable over time, can operate in environments with high humidity (80%), and shows high selectivity.

Supplementary Materials: The following are available online at <http://www.mdpi.com/2076-3417/10/18/6251/s1>: Figure S1. Schematic layout of the gas sensor measuring module; Figure S2. Reproducibility of the CH₄ detection by the 1% CQDs@NiO sensor at 30 ppm; Text. Description of the assembled device.

Funding: This research received no external funding.

Acknowledgments: René Bakker, currently working at CINECA, Rome Italy, is gratefully acknowledged for helping assemble the sensor device.

Conflicts of Interest: The author declares no conflict of interest.

References

1. Boulart, C.; Mowlem, M.C.; Connelly, D.P.; Dutasta, J.-P.; German, C.R. A novel, low cost, high performance dissolved methane sensor for aqueous environments. *Opt. Express* **2008**, *16*, 12607–12617. [[CrossRef](#)] [[PubMed](#)]
2. Xie, G.; Sun, P.; Yan, X.; Du, X.; Jiang, Y. Fabrication of methane gas sensor by layer by-layer self-assembly of polyaniline/PdO ultra thin films on quartz crystal microbalance. *Sens Actuators B Chem.* **2010**, *145*, 373–377. [[CrossRef](#)]
3. Zhu, L.; Zeng, W. Room-temperature gas sensing of ZnO-based gas sensor: A review. *Sens. Actuat. A Phys.* **2017**, *267*, 242–261. [[CrossRef](#)]
4. Lee, H.; Kim, D.H. Direct methanol synthesis from methane in a plasma-catalyst hybrid system at low temperature using metal oxide-coated glass beads. *Sci. Rep.* **2018**, *8*, 9956. [[CrossRef](#)]
5. Jebreil Khadema, S.M.; Abdia, Y.; Darbari, S.; Ostovari, F. Investigating the effect of gas adsorption on the electromechanical and electrochemical behavior of graphene/ZnO structure, suitable for highly selective and sensitive gas sensors. *Curr. Appl. Phys.* **2014**, *14*, 1498–1503. [[CrossRef](#)]
6. Valentini, F.; Roscioli, D.; Carbone, M.; Conte, V.; Floris, B.; Palleschi, G.; Flammini, R.; Bauer, E.M.; Nasillo, G.; Caponetti, E. Oxidized graphene in ionic liquids for assembling chemically modified electrodes: A structural and electrochemical characterization study. *Anal. Chem.* **2012**, *84*, 5823–5831. [[CrossRef](#)]
7. Valentini, F.; Carbone, M.; Palleschi, G. Carbon nanostructured materials for applications in nano-medicine, cultural heritage, and electrochemical biosensors. *Anal. Bioanal. Chem.* **2013**, *405*, 451–465. [[CrossRef](#)]
8. Pungjunun, K.; Chaiyo, S.; Praphairaksit, N.; Siangproh, W.; Ortner, A.; Kalcher, K.; Chailapakul, O.; Mehmet, E. Electrochemical detection of NO_x gas based on disposable paper-based analytical device using a copper nanoparticles-modified screen-printed graphene electrode. *Biosens. Bioelectron.* **2019**, *143*, 111606. [[CrossRef](#)]
9. Valentini, F.; Carbone, M.; Palleschi, G. Graphene oxide nanoribbons (GNO), reduced graphene nanoribbons (GNR), and multi-layers of oxidized graphene functionalized with ionic liquids (GO-IL) for assembly of miniaturized electrochemical devices. *Anal. Bioanal. Chem.* **2013**, *405*, 3449–3474. [[CrossRef](#)]
10. Zainal, P.N.S.; Ahmad, S.A.A.; Ngee, L.H. Surface Modification of Screen-Printed Carbon Electrode (SPCE) with Calixarene-Functionalized Electrochemically Reduced Graphene Oxide (ERGO/C4) in the Electrochemical Detection of Anthracene. *J. Electrochem. Soc.* **2019**, *166*, B110. [[CrossRef](#)]
11. Valentini, F.; Roscioli, D.; Carbone, M.; Conte, V.; Floris, B.; Bauer, E.M.; Ditaranto, N.; Sabbatini, L.; Caponetti, E.; Chillura-Martino, D. Graphene and ionic liquids new gel paste electrodes for caffeic acid quantification. *Sens. Actuat. B Chem.* **2015**, *212*, 248–255. [[CrossRef](#)]
12. Valentini, F.; Ciambella, E.; Boaretto, A.; Rizzitelli, G.; Carbone, M.; Conte, V.; Cataldo, F.; Russo, V.; Casari, C.S.; Chillura-Martino, D.F.; et al. Sensor Properties of Pristine and Functionalized Carbon Nanohorns. *Electroanalysis* **2016**, *28*, 2489–2499. [[CrossRef](#)]
13. Sekhar, P.K.; Kysar, J.; Brosha, E.L.; Kreller, C. Development and testing of an electrochemical methane sensor. *Sens. Actuat. B* **2016**, *228*, 162–167. [[CrossRef](#)]
14. Chaiyo, S.; Jampasa, S.; Thongchue, N.; Mehmeti, E.; Siangproh, W.; Chailapakul, O.; Kalcher, K. Wide electrochemical window of screen-printed electrode for determination of rapamycin using ionic liquid/graphene composites. *Microchim. Acta* **2020**, *187*, 245. [[CrossRef](#)] [[PubMed](#)]
15. Qiao, J.; Tang, S.; Tian, Y.; Shuang, S.; Dong, C.; Choi, M.M.F. Electro-catalytic oxidation of methane at multi-walled carbon nanotubes-Nafion/nickel hydroxide modified nickel electrode. *Sens. Actuat. B Chem.* **2009**, *138*, 402–407. [[CrossRef](#)]
16. Lee, I.; Akbar, S.A.; Dutta, P.K. High temperature potentiometric carbon dioxide sensor with minimal interference to humidity. *Sens. Actuat. B* **2009**, *142*, 337–341. [[CrossRef](#)]
17. Zhou, Q.; Lu, Z.; Wei, Z.; Xu, L.; Gui, Y.; Chen, W. Hydrothermal Synthesis of Hierarchical Ultrathin NiO Nanoflakes for High-Performance CH₄ Sensing. *Front. Chem* **2018**, *6*, 194. [[CrossRef](#)]

18. Carbone, M.; Bauer, E.M.; Micheli, L.; Missori, M. NiO morphology dependent optical and electrochemical properties. *Colloid. Surf. A* **2017**, *532*, 178–182. [[CrossRef](#)]
19. Carbone, M.; Micheli, L.; Nesticò, A.; Bellucci, N.; Palleschi, G. Enhanced performances of sensors based on screen printed electrodes modified with nanosized NiO particles. *Electrochim. Acta* **2017**, *246*, 580–587. [[CrossRef](#)]
20. Carbone, M.; Missori, M.; Micheli, L.; Tagliatesta, P.; Bauer, E.M. NiO Pseudocapacitance and Optical Properties: Does the Shape Win? *Materials* **2020**, *13*, 1417. [[CrossRef](#)]
21. Carbone, M. Cu-Zn-Co nanosized mixed oxides prepared from hydroxycarbonate precursors. *J. Alloy. Compd.* **2016**, *688*, 202–209. [[CrossRef](#)]
22. Carbone, M.; Briancesco, R.; Bonadonna, L. Antimicrobial power of Cu/Zn mixed oxide nanoparticles to Escherichia coli. *Environ. Nanotechnol. Monit. Manag.* **2017**, *7*, 97–102.
23. Carbone, M. Zn defective ZnCo₂O₄ nanorods as high capacity anode for lithium ion batteries. *J. Electroanal. Chem.* **2018**, *815*, 151–157. [[CrossRef](#)]
24. Wang, J.; Zeng, W.; Wang, Z. Assembly of 2D nanosheets into 3D flower-like NiO: Synthesis and the influence of petal thickness on gas-sensing properties. *Ceram. Int.* **2016**, *42*, 4567–4573. [[CrossRef](#)]
25. Gagaoudakis, E.; Michail, G.; Kampylafka, V.; Tsagaraki, K.; Aperathitis, E.; Moschovis, K.; Binas, V.; Kiriakidis, G. Room Temperature p-Type NiO Nanostructure Thin Film Sensor for Hydrogen and Methane Detection. *Sens. Lett.* **2017**, *15*, 1–5. [[CrossRef](#)]
26. Zhao, C.; Fu, J.; Zhang, Z.; Xie, E. Enhanced ethanol sensing performance of porous ultrathin NiO nanosheets with neck-connected networks. *RCS Adv.* **2013**, *3*, 4018–4023. [[CrossRef](#)]
27. Carbone, M.; Tagliatesta, P. NiO grained-flowers and nanoparticles for ethanol sensing. *Materials* **2020**, *13*, 1880. [[CrossRef](#)]
28. Zhang, D.; Chang, H.; Li, P.; Liu, R. Characterization of nickel oxide decorated-reduced graphene oxide nanocomposite and its sensing properties toward methane gas detection. *J. Mater. Sci. Mater. Electron.* **2016**, *27*, 723–730. [[CrossRef](#)]
29. Nakate, U.T.; Lee, G.H.; Ahmad, R.; Patil, P.; Bhopate, P.; Hahn, Y.B.; Yu, Y.T.; Suh, E.-K. Hydrothermal synthesis of p-type nanocrystalline NiO nanoplates for high response and low concentration hydrogen gas sensor application. *Ceram. Int.* **2018**, *44*, 15721–15729. [[CrossRef](#)]
30. Wei, Z.; Zhou, Q.; Wang, J.; Gui, Y.; Zeng, W. A novel porous NiO nanosheet and its H₂ sensing performance. *Mater. Lett.* **2019**, *245*, 166–169. [[CrossRef](#)]
31. Wu, C.-H.; Zhu, Z.; Chang, H.-M.; Jiang, Z.-X.; Hsieh, C.Y.; Wu, R.-J. Pt@NiO core-shell nanostructure for a hydrogen gas sensor. *J. Alloy. Compd.* **2020**, *814*, 151815. [[CrossRef](#)]
32. Wilson, R.L.; Simion, C.E.; Stanoiu, A.; Taylor, A.; Guldin, S.; Covington, J.A.; Carmalt, C.J.; Blackman, C.S. Humidity-Tolerant Ultrathin NiO Gas-Sensing Films. *ACS Sens.* **2020**, *5*, 1389–1397. [[CrossRef](#)] [[PubMed](#)]
33. Yang, M.; Lu, J.; Wang, X.; Zhang, H.; Chen, F.; Sun, J.; Yang, J.; Sun, Y. Acetone sensors with high stability to humidity changes based on Ru-doped NiO flower-like microspheres. *Sens. Actuat. B* **2020**, *313*, 127965. [[CrossRef](#)]
34. Xu, Y.; Fan, Y.; Tian, X.; Liang, Q.; Liu, X.; Sun, Y. P-p heterojunction composite of NiFe₂O₄ nanoparticles-decorated NiO nanosheets for acetone gas detection. *Mater. Lett.* **2020**, *270*, 127728. [[CrossRef](#)]
35. Liu, T.; Yu, Z.; Liu, Y.; Gao, J.; Wang, X.; Suo, H.; Yang, X.; Zhao, C.; Liu, F. Gas sensor based on Ni foam: SnO₂-decorated NiO for Toluene detection. *Sens. Actuat. B* **2020**, *318*, 128167. [[CrossRef](#)]
36. Xu, Y.; Tian, X.; Fan, Y.; Sun, Y. A formaldehyde gas sensor with improved gas response and sub-ppm level detection limit based on NiO/NiFe₂O₄ composite nanotetrahedrons. *Sens. Actuat. B* **2020**, *309*, 127719. [[CrossRef](#)]
37. Bai, S.; Han, J.; Han, N.; Zhang, K.; Sun, J.; Sun, L.; Luo, R.; Li, D.; Chen, A. An α-Fe₂O₃/NiO p-n hierarchical heterojunction for the sensitive detection of triethylamine. *Inorg. Chem. Front.* **2020**, *7*, 1532–1539. [[CrossRef](#)]
38. Qiu, L.; Zhang, S.; Huang, J.; Wang, C.; Zhao, R.; Qu, F.; Wang, P.; Yang, M. Highly selective and sensitive xylene sensors based on Nb-doped NiO nanosheets. *Sens. Actuat. B* **2020**, *308*, 127520. [[CrossRef](#)]
39. Liu, T.; Xu, L.; Wang, X.; Li, Q.; Cui, Q.; Suo, H.; Zhao, C. A simple dip-coating method of SnO₂-NiO composite thin film on a ceramic tube substrate for methanol sensing. *Crystals* **2019**, *9*, 621. [[CrossRef](#)]
40. Su, C.; Zhang, L.; Han, Y.; Ren, C.; Chen, X.; Hu, J.; Zeng, M.; Hu, N.; Su, Y.; Zhou, Z.; et al. Controllable synthesis of crescent-shaped porous NiO nanoplates for conductometric ethanol gas sensors. *Sens. Actuat. B* **2019**, *296*, 126642. [[CrossRef](#)]

41. Wang, C.; Cheng, X.; Zhou, X.; Sun, P.; Hu, X.; Shimano, K.; Lu, G.; Yamazo, N. Hierarchical α -Fe₂O₃/NiO Composites with a Hollow Structure for a Gas Sensor. *ACS Appl. Mater. Interfaces* **2014**, *6*, 12031–12037. [[CrossRef](#)] [[PubMed](#)]
42. Yao, L.; Li, Y.; Ran, Y.; Yang, Y.; Zhao, R.; Su, L.; Kong, Y.; Ma, D.; Chen, Y.; Wang, Y. Construction of novel Pd-SnO₂ composite nanoporous structure as a high-response sensor for methane gas. *J. Alloy. Compd.* **2020**, *826*, 154063. [[CrossRef](#)]
43. Xue, D.; Wang, P.; Zhang, Z.; Wang, Y. Enhanced methane sensing property of flower-like SnO₂ doped by Pt nanoparticles: A combined experimental and first-principle study. *Sens. Actuat. B* **2019**, *296*, 126710. [[CrossRef](#)]
44. Navazani, S.; Shokufar, A.; Hassanisadi, M.; Askrieh, M.; Di Carlo, A.; Agresti, A. Facile synthesis of a SnO₂@rGO nanohybrid and optimization of its methane-sensing parameters. *Talanta* **2018**, *181*, 422–430. [[CrossRef](#)] [[PubMed](#)]
45. Zhang, S.; Li, Y.; Sun, G.; Zhang, B.; Wang, Y.; Cao, J.; Zhang, Z. Enhanced methane sensing properties of porous NiO nanosheets by decorating with SnO₂. *Sens. Actuat. B* **2019**, *288*, 373–382. [[CrossRef](#)]
46. Dong, Y.; Shao, J.; Chen, C.; Li, H.; Wang, R.; Chi, Y.; Lin, X.; Chen, G. Blue luminescent graphene quantum dots and graphene oxide prepared by tuning the carbonization degree of citric acid. *Carbon* **2012**, *50*, 4738–4743. [[CrossRef](#)]
47. Zhou, M.; Zhou, Z.; Gong, A.; Zhang, Y.; Li, Q. Synthesis of highly photoluminescent carbon dots via citric acid and Tris for iron(III) ions sensors and bioimaging. *Talanta* **2015**, *143*, 107–113. [[CrossRef](#)]
48. Vaz, R.; Bettini, J.; Júnior, J.G.F.; Lima, E.D.S.; Botero, W.G.; Santos, J.C.C.; Schiavona, M.A.J. High luminescent carbon dots as an eco-friendly fluorescence sensor for Cr(VI) determination in water and soil samples. *Photoch. Photobiol. A* **2017**, *346*, 502–511. [[CrossRef](#)]
49. Mishra, R.K.; Upadhyay, S.B.; Kushwaha, A.; Kim, T.-H.; Murali, G.; Verma, R.; Srivastava, M.; Singh, J.; Sahay, P.P.; Lee, S.H. SnO₂ quantum dots decorated on RGO: A superior sensitive, selective and reproducible performance for a H₂ and LPG sensor. *Nanoscale* **2015**, *7*, 11971–11979. [[CrossRef](#)]
50. Bhattacharjee, L.; Manoharan, R.; Mohanta, K.; Bhattacharjee, R.R. Conducting carbon quantum dots—A nascent nanomaterial. *J. Mater. Chem. A* **2015**, *3*, 1580–1586. [[CrossRef](#)]
51. Wang, X.; Feng, Y.; Dong, P.; Huang, J. A Mini Review on Carbon Quantum Dots: Preparation, Properties, and Electrocatalytic Applications. *Front. Chem.* **2019**, *7*, 671. [[CrossRef](#)] [[PubMed](#)]
52. Caminiti, R.; Carbone, M.; Panero, S.; Sadun, C. Conductivity and structure of poly(ethylene glycol) complexes using energy dispersive X-ray diffraction. *J. Phys. Chem. B* **1999**, *103*, 10348–10355. [[CrossRef](#)]
53. JCPDS 22-1189.
54. Azim-Araghi, M.E.; Krier, A. Thin film (ClAlPc) phthalocyanine gas sensors. In *Selected Topics in Advanced Solid State and Fibre Optic Sensors*; Vaezi-Nejad, S.M., Ed.; The Institute of Engineering and Technology (IET): London, UK, 2000.
55. Wales, D.J.; Parker, R.M.; Gates, J.C.; Grossel, M.C.; Smith, P.G.R. An investigation into relative humidity measurement using analuminosilicate sol-gel thin film as the active layer in an integrated optical Bragg grating refractometer. *Sens. Actuat B* **2013**, *188*, 857–866. [[CrossRef](#)]
56. Kim, H.-J.; Lee, J.-H. Highly sensitive and selective gas sensors using p-type oxide semiconductors: Overview. *Sens. Actuat B* **2014**, *192*, 607–627. [[CrossRef](#)]
57. Kim, H.-J.; Choi, K.-I.; Kim, K.-M.; Na, C.W.; Lee, J.-H. Highly sensitive C₂H₅OH sensors using Fe-doped NiO hollow spheres. *Sens. Actuat B* **2012**, *171*, 1029–1037. [[CrossRef](#)]
58. Miller, D.R.; Akbar, S.A.; Morris, P. Nanoscale metal oxide-based heterojunctions for gas sensing: A review. *Sens. Actuat. B* **2014**, *204*, 250–272. [[CrossRef](#)]
59. Walker, J.M.; Akbar, S.A.; Morris, P.A. Synergistic effects in gas sensing semiconducting oxide nano-heterostructures: A review. *Sens. Actuat. B* **2019**, *286*, 624–640. [[CrossRef](#)]
60. Fu, J.; Zhao, C.; Zhang, J.; Peng, Y.; Xie, E. Enhanced Gas Sensing Performance of Electrospun Pt-functionalized NiO Nanotubes, with Chemical and Electronic Sensitization. *ACS Appl. Mater. Interfaces* **2013**, *5*, 7410–7416. [[CrossRef](#)]

